

Activation of Hematite Photoanodes for Solar Water Splitting: Effect of FTO Deformation

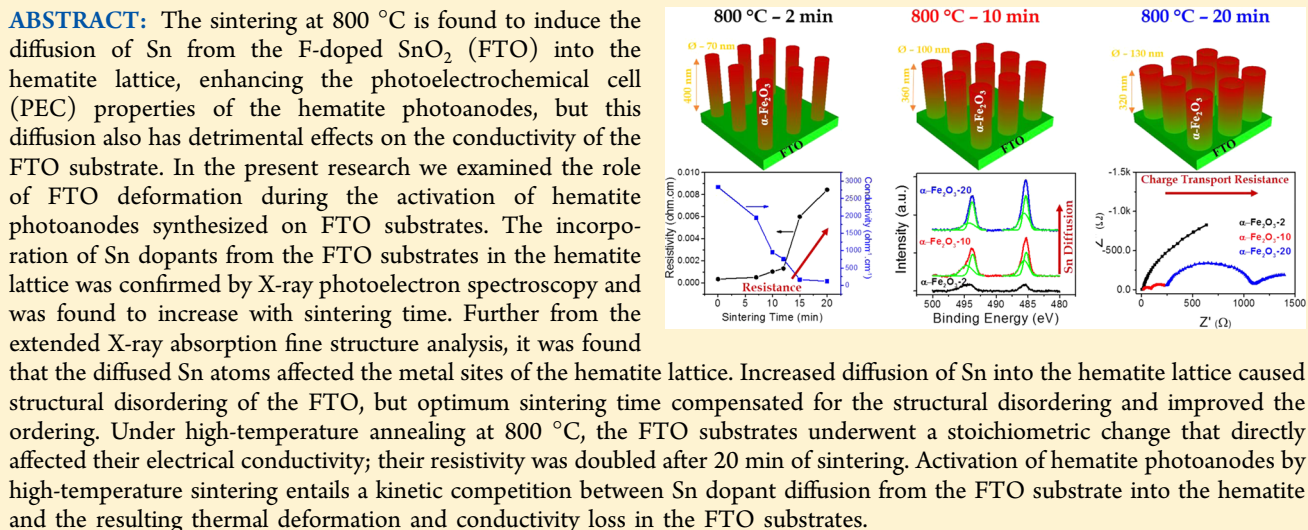
Alagappan Annamalai,[†] Arunprabaharan Subramanian,[†] Unseock Kang,[‡] Hyunwoong Park,[‡] Sun Hee Choi,[§] and Jum Suk Jang*,[†]

[†]Division of Biotechnology, Advanced Institute of Environmental and Bioresource Sciences, College of Environmental and Bioresource Sciences, Chonbuk National University, 79 Gobong-ro, Iksan 570–752, Korea

[‡]School of Energy Engineering, Kyungpook National University, 80 Daehakro, Bukgu, Daegu 702–701, Korea

[§]Pohang Accelerator Laboratory, Pohang University of Science and Technology, San 31 Hyoja Dong 319, Pohang 790–784, Korea

S Supporting Information



INTRODUCTION

Solar water splitting is an environmental friendly way of converting solar energy to hydrogen by photoelectrochemical means.¹ Honda and Fujishima first demonstrated photoelectrochemical water splitting in 1972, using TiO₂ as the photoanode,² and several important advancements have been achieved in the intervening 4 decades, including improvements to solar-to-hydrogen (STH) conversion efficiencies and developments that have lowered production costs for commercial applications.^{3–5} Numerous semiconductor metal oxides have been examined as photoanodes for photoelectrochemical water splitting, including TiO₂,⁶ ZnO,⁷ WO₃,⁸ BiVO₄,⁹ and Fe₂O₃.¹⁰ Among them, hematite (α -Fe₂O₃) is one of the most promising as a photoanode material for PECs, having a favorable bandgap of 2.2 eV, excellent chemical stability, and low cost.^{10,11} However, the application of hematite in PECs is limited by many factors such as its short hole diffusion length (2–4 nm), poor oxygen evolution kinetics, and very short excited-state lifetime.^{3,12} These poor optoelectronic properties can be overcome by using nanostructured hematite photoanodes¹³ and adding elemental doping;¹⁴ both of these strategies have been shown to improve photoactivity.¹⁰

Vertically aligned nanorods are an ideal hematite morphology for PEC applications because the thin nanorods can overcome hole transport limitations, while the high surface area and 1-D nanostructuring improve the surface and facilitate the transport of photoexcited electrons to the conducting substrates.⁴

Metal oxide semiconductor photoanodes are usually coated or deposited on a conducting substrate, which is used as a back contact for photoelectrochemical measurements.¹⁵ In most cases, transparent conducting oxides (TCOs) are preferred because they allow the use of either front- or backside illumination to characterize the photoanode.³ The TCO should form an ohmic contact with the semiconductor photoanode for effective charge transport and should have high carrier concentrations and mobilities as well as good optical transparency (>80%).⁴ For n-type photoanodes such as hematite, TCOs are used with a work function that is lower than that of the photoanode itself.¹⁰ Some of the most commonly used TCOs are FTO and Sn-doped In₂O₃ (ITO).¹⁶ FTO and ITO

Received: December 8, 2014

Revised: January 23, 2015

Published: January 26, 2015

having sheet resistances ranging from 8 to 30 Ω/sq are commercially available. Even though FTO is less conductive than ITO, FTO is presently the conducting substrate of choice because ITO is less thermal stable and less resistant to chemicals.¹⁶ Choosing TCOs for PEC applications becomes more difficult when postdeposition high-temperature sintering is required because the glass substrate upon which the TCO layers are deposited softens above $\sim 550\text{ }^\circ\text{C}$, inducing physical deformation.¹⁷ The conductivity of ITO decreases drastically when sintered above $350\text{ }^\circ\text{C}$,¹⁶ whereas FTO and ITO/FTO coatings are stable up to $\sim 800\text{ }^\circ\text{C}$ and may still have acceptable conductivities at higher temperatures provided that the sintering time is $< 30\text{ min}$.¹⁸ For higher temperatures or longer sintering times, noble-metal films (e.g., Pt films) should be used, but these might not allow transparency of the conducting substrate and thus may considerably worsen its optical properties.¹⁹

Vayssières et al. synthesized hematite nanorods on FTO substrates by a simple hydrothermal method;²⁰ however, their photoactivity is poor.¹³ Sivula et al.¹⁹ enhanced the photoactivity of these structures by sintering the hematite photoanodes at $800\text{ }^\circ\text{C}$; under this high-temperature sintering, Sn from the FTO substrates diffused into the hematite lattice. The incorporation of Sn was characterized by X-ray photoelectron spectroscopy. This intrinsic Sn doping into the hematite lattice when sintered at high temperature is termed the activation of hematite photoanodes.¹⁸ The improvement of activity by high-temperature sintering suggests that a minimum activation energy is required to induce the diffusion of Sn^{4+} cation impurities into the hematite lattice and to activate them as dopants.¹⁸ A drastic change in the diffusion coefficient of $^{55}\text{Fe}^{3+}$ isotopes in hematite²¹ as well as an increase in C3v crystal distortion²² were observed only after heating to $\sim 800\text{ }^\circ\text{C}$. These effects have been correlated to the increased absorption of photoanodes sintered at high temperature, suggesting that the lattice relaxation that occurs during sintering is an important contributor to the observed enhancement of hematite's optoelectronic properties.^{10,18} The general activation temperature of hematite has been reported to be $800\text{ }^\circ\text{C}$ for 20 min.¹⁷ There have been a few reports^{10,13,18,19} of studies on the activation of hematite photoanodes and the changes in the hematite photoanodes but none with respect to the systematic and detailed study on deformation of FTO substrates during the high-temperature sintering conditions. The changes in FTO substrates with high-temperature sintering are arguably the most important aspect as FTO substrates are widely used in most of the photovoltaic and photochemical devices owing to their superior optoelectronic properties. We report results concerning the characterization of FTO substrate deformation by high-temperature sintering, including the activation of hematite photoanodes. Sn diffusion into the hematite lattice was analyzed by means of X-ray photoelectron spectroscopy and was shown to increase with sintering time. Extended X-ray absorption fine structure (EXAFS) analysis was used to investigate the electronic and local structure of Fe within the hematite photoanodes and Sn within the FTO substrates after high-temperature sintering. The use of optimum sintering conditions is necessary to improve ordering because increasing the diffusion of Sn into the hematite lattice also increases its structural disorder. Activation of hematite photoanodes by high-temperature sintering entails a kinetic competition between Sn dopant diffusion from the FTO substrate into the hematite and the resulting thermal deformation and

conductivity loss in the FTO substrates. We discuss the factors affecting the photoactivity of the hematite photoanodes on FTO substrates sintered at $800\text{ }^\circ\text{C}$, considering that the sintering can also cause thermal deformation and conductivity loss in the FTO substrates. The deformation effects in FTO substrates with high-temperature sintering give us a better understanding with respect to various photoanodes, so that it can be tailored to suit different applications.

■ EXPERIMENTAL SECTION

Hematite 1-D nanostructures on FTO substrates were prepared by a simple hydrothermal method based on that in a previous report.²⁰ In a typical experiment, a piece of cleaned FTO substrate ($1\text{ cm} \times 2.5\text{ cm}$) was placed in a 20 mL vial containing an aqueous solution (10 mL) of 0.4 g $\text{FeCl}_3 \cdot 6\text{H}_2\text{O}$ and 0.85 g NaNO_3 at pH 1.5 (adjusted by HCl). The hydrothermal reaction was carried out at $100\text{ }^\circ\text{C}$ for 6 h. The FTO substrates were cooled to room temperature, were rinsed several times with distilled water, and were then dried at $60\text{ }^\circ\text{C}$. The substrates were then annealed at $550\text{ }^\circ\text{C}$ for 4 h to induce a phase transition from $\beta\text{-FeOOH}$ to pure $\alpha\text{-Fe}_2\text{O}_3$; then, these $\alpha\text{-Fe}_2\text{O}_3$ photoanodes were subjected to high-temperature sintering ($800\text{ }^\circ\text{C}$) for various periods of time.

X-ray diffraction (XRD) patterns were collected for all samples by using an X-ray diffractometer (Rigaku RINT 2500) with a $\text{CuK}\alpha$ radiation source. The surface morphologies of samples were analyzed by using field-emission scanning electron microscopy (FESEM, JEOL JSM 700F). X-ray photoelectron spectroscopy (XPS) was carried out by using an X-ray photoelectron spectrometer (ULVAC-PHI, Japan). The local structures of FTO substrates and hematite photoanodes were investigated by means of X-ray absorption fine structure (XAFS) analysis. X-ray measurements were performed on the 7D beamline of the Pohang Light Source II of the Pohang Accelerator Laboratory (PLS-II, 3.0 GeV). The synchrotron radiation was monochromatized by using a Si(111) double-crystal monochromator. The spectra for the Sn K-edge ($E_0 = 29\,200\text{ eV}$) of the FTO samples and the Fe K-edge ($E_0 = 7112\text{ eV}$) of the hematite photoanodes that had been sintered at $800\text{ }^\circ\text{C}$ for different times were both collected at room temperature using a fluorescence mode. The incident beam was not detuned for the Sn K-edge measurement and was detuned by 30% for the Fe K-edge measurement to minimize contamination by higher harmonics. The intensity of the incident beam was monitored by using an IC SPEC ionization chamber, which was filled with N_2 and with He, respectively, for the Sn and Fe K-edge experiments. Fluorescence signals from the samples were measured by a passivated implanted planar silicon detector attached to a sample chamber through which He was flowed. The fluorescence data obtained were analyzed by ATHENA of the IFEFFIT suite of programs.²³ All photoelectrochemical measurements were carried out in 1 M NaOH electrolyte (pH 13.8) using a Ivium CompactStat potentiostat with a platinum coil as the counter electrode and Ag/AgCl as the reference electrode. Photocurrent–potential (J – V) curves were collected over the range from 0.3 to 1.7 V versus a reversible hydrogen electrode using the sweep rate of 50 mV s^{-1} . Impedance spectroscopy measurements were performed by using an impedance analyzer (Ivumstat). Impedance spectra were measured over the frequency range of 1×10^{-2} to $3 \times 10^6\text{ Hz}$ at $25\text{ }^\circ\text{C}$ under open-circuit conditions with the amplitude of 10 mV and under the bias illumination of 100 mW cm^{-2} . Hereafter, hematite photo-

anodes sintered at 800 °C for 2, 10, and 20 min are, respectively, termed $\alpha\text{-Fe}_2\text{O}_3\text{-}2$, $\alpha\text{-Fe}_2\text{O}_3\text{-}10$, and $\alpha\text{-Fe}_2\text{O}_3\text{-}20$.

RESULTS AND DISCUSSION

X-ray patterns were collected for FTO substrates sintered at 800 °C for 0, 2, 10, and 20 min (Figure 1); all of the X-ray

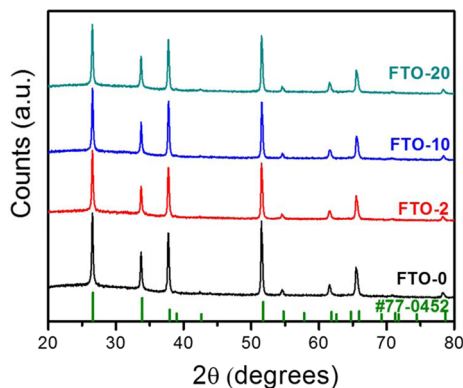


Figure 1. X-ray diffraction patterns of FTO substrates sintered at 800 °C for 0, 2, 10, and 20 min (SnO₂: JCPDS #77-0452).

diffraction peaks for pristine FTO substrate and those sintered at high-temperature (800 °C) were indexed to the XRD patterns of the SnO₂ of FTO (JCPDS # 77-0452). The XRD patterns showed no noticeable difference in the crystal structure of the FTO substrates sintered for different times. The surface morphology of the FTO films was studied by using FESEM, as shown in Figure 2a–c. The grain size and thickness of the FTO

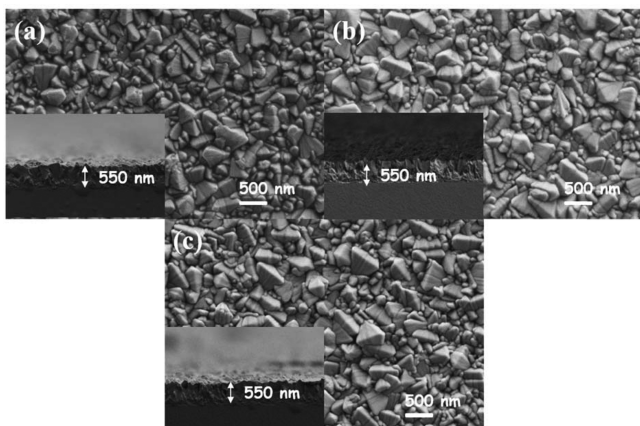


Figure 2. FESEM images of FTO substrates sintered at 800 °C for (a) 2, (b) 10, and (c) 20 min; (insets) thicknesses of the sintered FTO substrates.

substrates remained the same regardless of the sintering time at 800 °C. However, deformation of the FTO substrates was observed in the sample sintered for 20 min because the glass in the FTO substrate undergoes melting above 700 °C.¹⁷ The electrical properties such as resistivity and conductivity of the sintered FTO substrates were investigated by Hall effect measurements. Fluorine atoms in the SnO₂ matrix of the FTO substrate are solely responsible for its n-type conductive property, which mainly depends on stoichiometry, and this stoichiometry is strongly influenced by sintering temperature.^{10,16} The resistivity was observed to increase with increased sintering time at 800 °C (Figure 3). At high

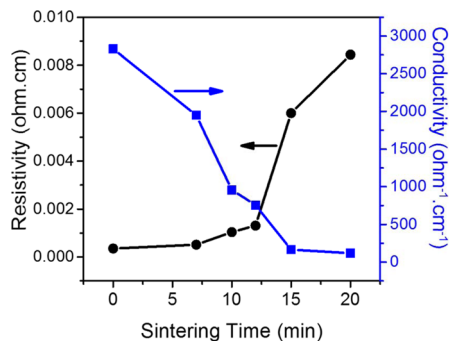


Figure 3. Hall effect measurements of FTO substrates sintered at 800 °C for 2, 10, and 20 min.

temperature such as 800 °C, the FTO substrates undergo a stoichiometric change that directly affects the electrical conductivity (Table S1 in the SI), resulting, for example, in the doubling of resistivity that was observed after 20 min of sintering. The observed conductivity changes affected the overall device performance, which will be discussed later.

The nanorod photoanodes were sintered at 800 °C to induce the activation of hematite photoanodes by diffusion of Sn from the FTO layer into the hematite.¹⁸ In X-ray diffractograms of hematite photoanodes sintered at 800 °C from 2 to 20 min, all hematite photoanodes displayed similar patterns with a predominant (110) diffraction peak (Figure 4), without any

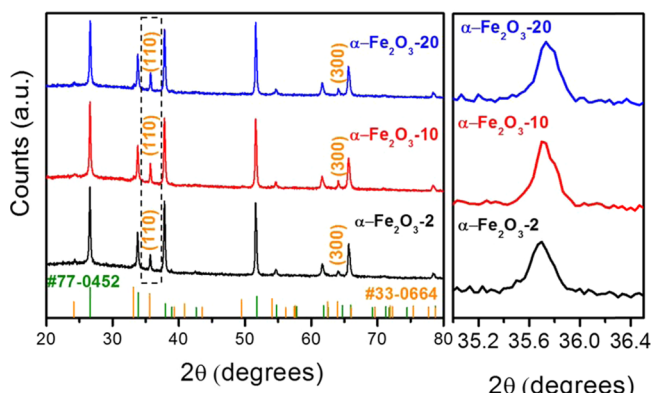


Figure 4. X-ray diffraction patterns of hematite photoanodes on FTO substrates sintered at 800 °C for 2, 10, and 20 min. (SnO₂: JCPDS #77-0452; $\alpha\text{-Fe}_2\text{O}_3$: JCPDS #33-0664).

change in structure or crystal phase of the hematite nanorods; the (110) orientation has been suggested as a preferential orientation for electron transport in hematite photoanodes.¹⁰ As the sintering time was increased, the resulting diffraction peaks became sharper, with a decrease in full width at half-maximum (fwhm) resulting from a significant increase in crystallite size. The effects of sintering time on the morphology of the hematite photoanodes were examined by using scanning electron microscopy. From FESEM images, the average diameter (measured from 50 different spots) of the hematite nanorods increases from 70 to 130 nm (Figure 5a–c), while the average length decreases from 400 to 320 nm (Figure 5d–f), with increasing the sintering time from 2 to 20 min at 800 °C, which could be explained by enhanced grain growth at high-temperature sintering. Initially, the hematite nanorods were thin and irregular in shape; hematite photoanodes sintered at 800 °C for 2 min appeared very similar to photoanodes

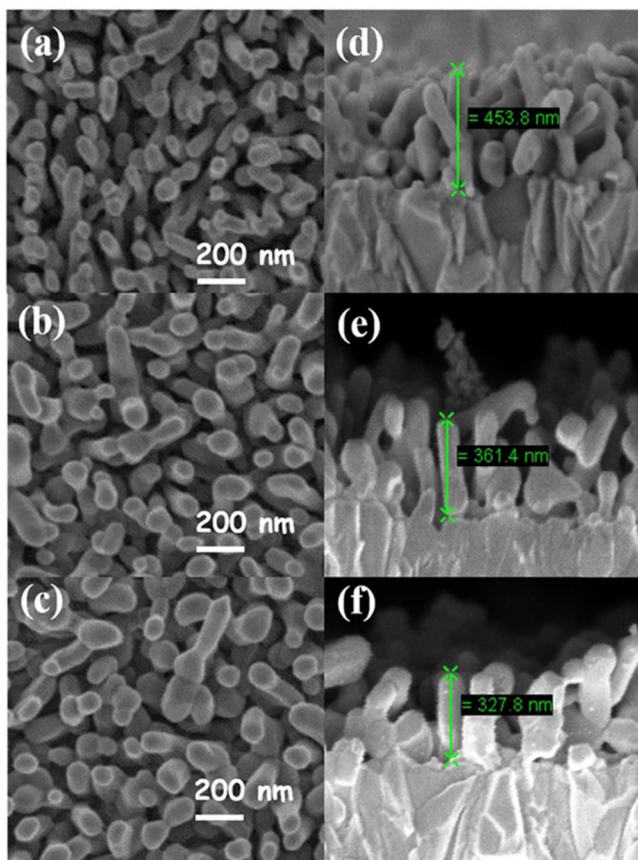


Figure 5. FESEM images of hematite photoanodes on FTO substrates sintered at 800 °C for (a) 2, (b) 10, and (c) 20 min and their respective cross-section images in panels d–f, respectively.

sintered at 550 °C. From Figure S1 in the SI; however, after 10 min at 800 °C a change of morphology is observed, including grain ripening, resulting in coalesced features with very smooth surfaces as reported.¹⁷ Heating at 800 °C for more than 10 min produced a similar morphology, although the average feature size was increased with sintering time possibly due to aggregation induced by the prolonged sintering process.¹⁷

To confirm the incorporation of Sn that diffused from the FTO substrate into the hematite nanorods, XPS analyses were performed; detailed analysis of the Fe 2p (Figure 6b) and O 1s (Figure 6c) regions in a full survey scan (Figure 6a) revealed no significant change with respect to sintering time. However, Sn was detected on hematite photoanodes even after only 2 min of sintering, and the intensity of the Sn 3d XPS peak increased with sintering time (Figure 6d). A more detailed individual Sn 3d XPS spectrum of hematite photoanodes sintered at 800 °C exhibited two peaks around 495.1 and 486.4 eV, corresponding, respectively, to the Sn 3d_{3/2} and Sn 3d_{5/2} peaks.^{13,18} The amount of Sn diffused into the hematite lattice was the lowest for samples sintered for 2 min, and as the sintering time was increased the Sn diffusion also increased: when the sintering time was increased to 10 min, more Sn was incorporated, and the hematite photoanodes sintered for 20 min showed the highest amount of Sn diffused into the hematite lattice, which caused severe deformation to the FTO substrate. The Sn detected in the hematite photoanodes sintered at 800 °C was found to originate from the FTO substrates, as reported previously.^{13,18,19} With increasing sintering time, the Sn 3d_{3/2} and Sn 3d_{5/2} peaks shifted to lower binding energies. Because the electronegativity of Sn (1.96) is higher than that of Fe (1.83), when Sn is incorporated into the FeO matrix, the Sn 3d_{3/2} and Sn 3d_{5/2} peaks shift to lower binding energies.²⁴ The

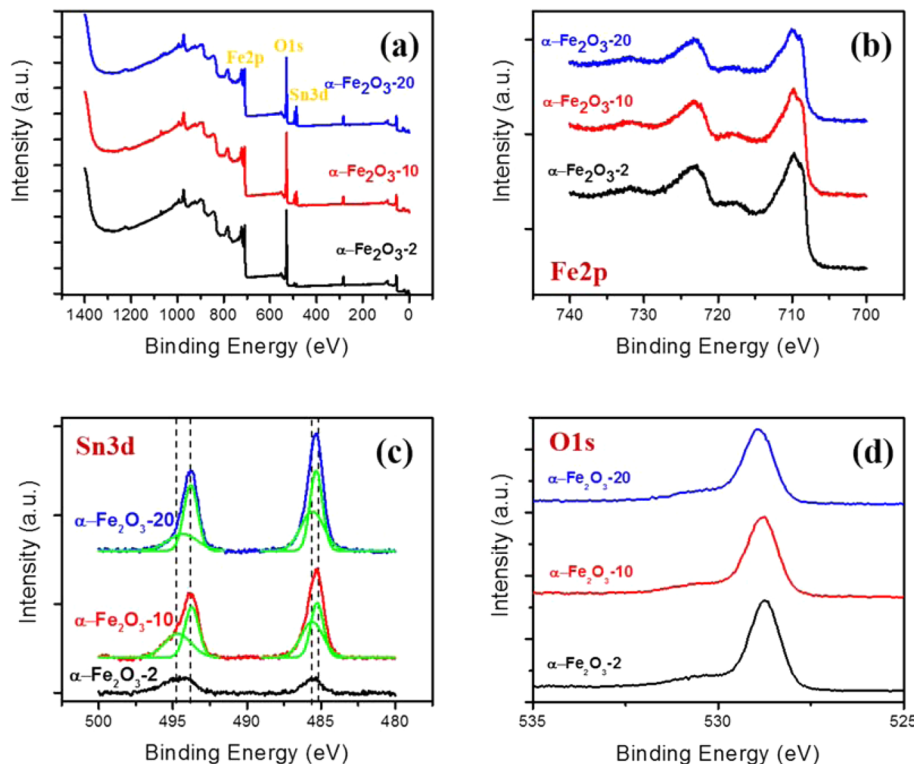


Figure 6. XPS spectra recorded from hematite photoanodes on FTO substrates sintered at 800 °C for 2, 10, and 20 min: (a) full scan, (b) Fe 2p, (c) Sn 3d, and (d) O 1s.

present results confirmed that diffused Sn was present in all hematite photoanodes sintered at 800 °C (Table S2 in the SI). Although the hematite photoanodes sintered for 20 min contained the most diffused Sn, the prolonged sintering at 800 °C severely deformed the glass substrate, causing the FTO layer to become insulating. That is to say, although 800 °C sintering favors Sn diffusion from the FTO substrate into the hematite nanostructure, it also changes the stoichiometry of the FTO substrate, substantially degrading the conductivity of the FTO substrate.

Photoelectrochemical performance was measured by using 1.0 M NaOH as the electrolyte and 800 °C sintered hematite nanorods on FTO substrates as photoanodes, as shown in Figure 7. For hematite photoanodes sintered for 2 min at 800

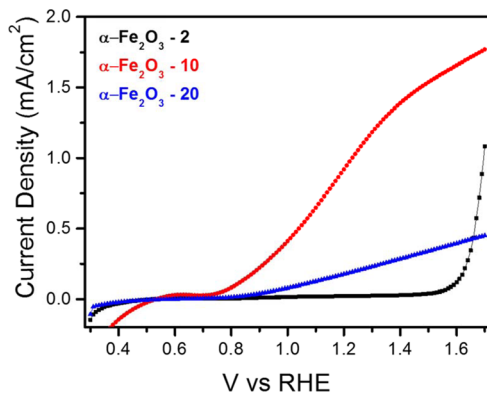


Figure 7. Photocurrent–potential (J – V) curves for the PEC water oxidation reaction with hematite photoanodes on FTO substrates sintered at 800 °C for 2, 10, and 20 min using 1 M NaOH electrolyte under 1 sun standard illumination conditions.

°C, no photoactivity was observed (i.e., the dark current and the photocurrent were the same), very similar to the lack of activity reported for photoanodes sintered at 550 °C,^{13,18,19} because little Sn diffusion occurred after this brief sintering. Significantly, the photocurrent of hematite photoanodes dramatically increased with sintering time at 800 °C (Figure S2 in the SI). The photocurrent improved steadily with increased time until the optimum time of 10 min, owing to increased Sn diffusion into the hematite lattice; the sudden drop in photocurrent for hematite photoanodes sintered for longer than 10 min can be attributed to deformation of the FTO substrate, increasing its resistivity. In other words, in our experiments, the hematite nanorods on FTO substrates sintered at 800 °C for 10 min yielded the highest photocurrent of 0.98 mA/cm² at 1.23 V versus a reversible hydrogen electrode, whereas increased sintering time at 800 °C caused severe deformation of the glass substrate, causing the FTO layer to become insulating. This result suggested a strong correlation between Sn diffusion and the PEC performance of hematite nanostructures.

To confirm the change in stoichiometry of sintered FTO substrates, we performed XPS analyses. The fluorine content of the FTO was below the XPS detection limit (Figure S1 in the SI). Because the XPS analyses of FTO substrates were inconclusive, we further carried out X-ray absorption near edge structure (XANES) and EXAFS analyses to evaluate the changes in the stoichiometry of the FTO substrates. Sn K-edge XANES spectra of all annealed FTO substrates had the same spectral features as the reference SnO_2 spectrum, regardless of

annealing time (Figure 8a). Similarly, Fe K-edge XANES spectra of annealed hematite photoanodes were exactly the

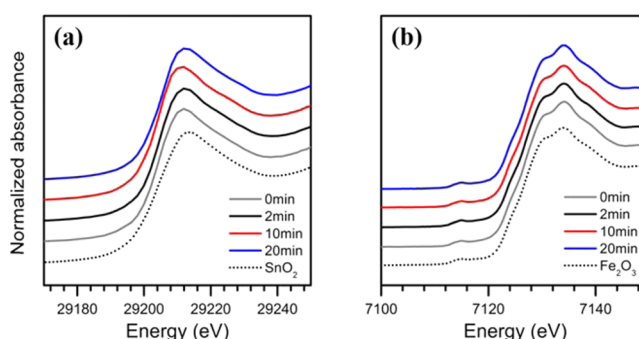


Figure 8. XANES spectra for (a) Sn K-edge of FTO substrates and (b) Fe K-edge of hematite photoanodes, both of which were sintered at 800 °C for 0, 2, 10, and 20 min.

same as that of reference $\alpha\text{-Fe}_2\text{O}_3$: a pre-edge peak denoting a quadrupole transition of $1s \rightarrow 3d$ was observed at 7115 eV in every spectrum, and the absorption rising feature and energy position were also the same in every spectrum (Figure 8b). The oxidation states of Sn and Fe in the samples were preserved despite the high-temperature sintering. The local structure of neighboring atoms around an absorbing atom was probed by means of EXAFS. Fourier-transformed spectra of EXAFS functions were prepared for the Sn K-edge of FTO substrates (Figure 9a) and the Fe K-edge of hematite photoanodes (Figure 9b) sintered at 800 °C for various periods. The Sn spectra exhibited two major peaks at 0.8 to 2.0 and 3.1 to 4.2 Å; the former denoted 5 Fe–O scatterings at 2.05 Å bond distance, and the latter was associated with 2 Sn–Sn at 3.18 Å, 3 Fe–O at 3.59 Å, 8 Sn–Sn at 3.70 Å, and 4 Sn–O at 3.79 Å.

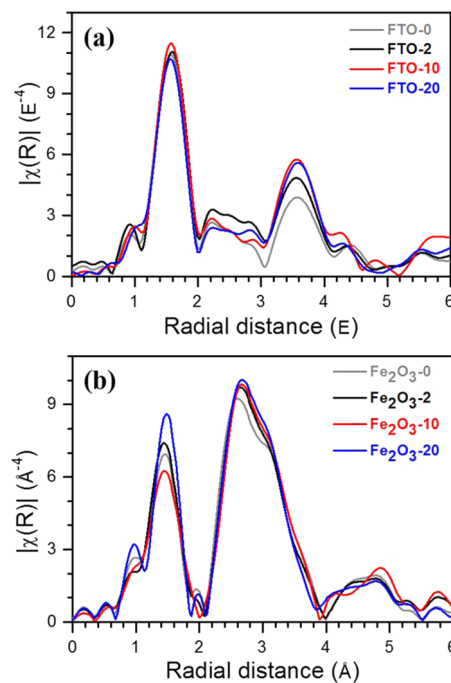


Figure 9. k^3 -weighted Fourier transforms for (a) Sn K-edge EXAFS of FTO substrates and (b) Fe K-edge EXAFS of hematite photoanodes, both of which were sintered at 800 °C for 0, 2, 10, and 20 min.

The identification was enabled by FEFF calculations using the known crystal structure of SnO_2 .^{25,26} With increasing sintering time, the second peak at 3.1 to 4.2 Å became more intense, indicating that the annealing enhanced ordering at distant shells. However, the intensity of the first peak increased in the sequence of 20 min < 0 min ≈ 2 min < 10 min. The 10 min annealing enhanced the ordering of the shortest Sn–O bond, but more annealing (20 min) caused deformation in the short-distance bonds. In the Fourier transform spectrum of the Fe K-edge of hematite photoanodes, two distinct peaks were observed at 0.8 to 2.0 and 2.1 to 3.9 Å (Figure 9b.) The intensity of the second peak at 2.1 to 3.9 Å was slightly increased for the samples sintered at 800 °C relative to the as-prepared sample. This peak was composed of complicated Fe–Fe and Fe–O scatterings (1 Fe–Fe at 2.90 Å, 3 Fe–Fe at 2.97 Å, 3 Fe–Fe at 3.36 Å, 3 Fe–O at 3.40 Å, 3 Fe–O at 3.60 Å, 6 Fe–Fe at 3.70 Å, and 3 Fe–O at 3.78 Å).²⁷ As Sn from the FTO substrate diffused into the hematite nanorods, the Sn atoms became located in metal sites of the hematite lattice. The heavier Sn atoms then induced stronger backscattering in absorber–neighbor scattering events relative to the original Fe atom, thereby strengthening the EXAFS signal. The peak at 0.8 to 2.0 Å denoting the shortest Fe–O bond increased in the sequence of 10 min < 0 min ≈ 2 min < 20 min, opposite to the results for Sn EXAFS. With increased diffusion of Sn into hematite lattice, the ordering worsened, but sufficient sintering time (10 min) compensated for the structural distortion and improved the ordering.

Impedance measurements were carried out to characterize the major internal charge transfer resistances across the TCO–photoanode and photoanode–electrolyte interfaces of hematite photoanodes, both of bare anodes and those sintered at 800 °C. Electrochemical impedance spectroscopy (EIS) is a steady-state method used for measuring the current response to the application of an AC voltage as a function of frequency.²⁸ Figure 10 shows the Nyquist plots of 800 °C sintered hematite

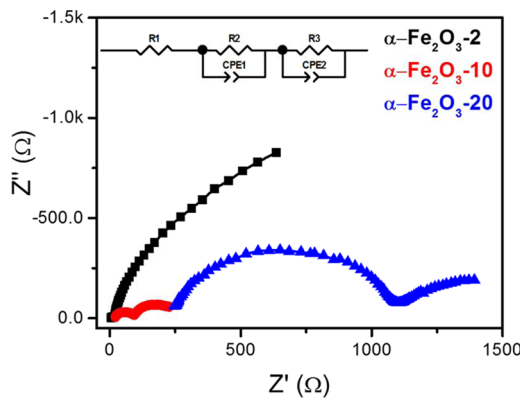


Figure 10. Nyquist plots of hematite photoanodes on FTO substrates sintered at 800 °C for 2, 10, and 20 min using 1 M NaOH electrolyte under 1 sun standard illumination conditions.

nanorods on FTO substrates as photoanodes from electrochemical impedance under standard illumination conditions with two semicircles. From Nyquist plots and equivalent circuit, R_s is the series resistance, which includes mainly the sheet resistance of the FTO substrate and the external contact resistance of the cell (e.g., wire connections and alligator clips). The parallel $R_{\text{CT}1}$ and CPE_1 elements characterize the charge-transfer resistance and the double-layer capacitance at the

FTO/ α -Fe₂O₃ interface, whereas $R_{\text{CT}2}$ and CPE_2 , respectively, characterize the charge-transport resistance of α -Fe₂O₃ and the double-layer capacitance of the α -Fe₂O₃/electrolyte interface.²⁹ Table 1 lists fitting results for hematite photoanodes

Table 1. Output of the Equivalent Circuit Model Based on Nyquist Plots, for Hematite Photoanodes Annealed at 800 °C for 2, 10, and 20 min Using 1 M NaOH under 1 Sun Illumination Conditions

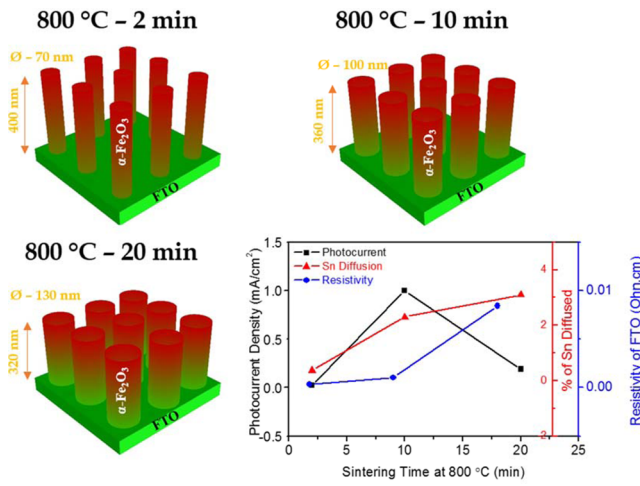
(R/Ω) (CPE/F)	α -Fe ₂ O ₃ -2	α -Fe ₂ O ₃ -10	α -Fe ₂ O ₃ -20
R_s	4.4	19.1	227.7
$R_{\text{CT}1}$	13.5	76.4	870.5
CPE_1	2.1×10^{-6}	7.7×10^{-6}	7.2×10^{-8}
$R_{\text{CT}2}$	2004	150.7	581.6
CPE_2	1.3×10^{-5}	2.2×10^{-5}	7.3×10^{-5}

sintered at 800 °C; R_s and $R_{\text{CT}1}$ increased from 4 to 228 and from 14 to 871 with increased sintering time, respectively, whereas $R_{\text{CT}2}$ decreased from 2004 to 150 Ω and then increased to 582 Ω with increased sintering time from 2 to 20 min. With increasing sintering time, the starting point of the semicircles, R_s , the series resistance,³⁰ of the hematite photoanodes was found to increase. The deformation of the FTO substrate at 800 °C caused the overall resistance to increase at the highest sintering time; the increase in FTO resistivity upon increased sintering time was confirmed from the Hall effect measurements and EIS measurements (Figure S3 in the SI). The PEC performance was well-correlated with changes in Sn diffusion and the EIS data. It was found that the FTO/ α -Fe₂O₃ interface charge-transport resistance, $R_{\text{CT}1}$, increased with sintering time as a result of the changing stoichiometry and increasing FTO resistivity. $R_{\text{CT}2}$ represents the complex charge-transfer behavior occurring in α -Fe₂O₃ and the α -Fe₂O₃/electrolyte interface.²⁹ The charge-transport resistance $R_{\text{CT}2}$ decreased with increased sintering time, from 2000 to 150 Ω (92%) due to an increase in the number of charge carriers as Sn diffused into the hematite lattice from 2 to 10 min. When an optimum amount of Sn diffuses into the hematite lattice, high carrier conductivities can be attained,¹³ but as the sintering time was increased further from 10 to 20 min, $R_{\text{CT}2}$ increased again to 581 Ω. This was because as the sintering time was increased, the hematite's resistivity was affected by excessive Sn doping and the FTO substrate started to deteriorate, thereby decreasing the mobility of charge carriers and thus increasing $R_{\text{CT}2}$ relative to that of the hematite photoanodes sintered for the optimum 10 min. On the basis of the previous results we confirmed that Sn diffusion from the FTO substrates into the hematite lattice is solely responsible for the enhanced photoactivity of hematite photoanodes (Scheme 1). There is a trade-off between Sn diffusion into the hematite lattice and loss of Sn in the original FTO substrate, which considerably degrades the FTO layer and makes it insulating. Further studies will be necessary to fully elucidate the deformation phenomenon.

CONCLUSIONS

High-temperature sintering is used to activate hematite photoanodes on FTO substrates, and herein the effect of sintering time upon FTO deformation was studied for the first time in detail, by means of a combination of Hall effect measurements, XPS, EXAFS, and photoelectrochemical characterizations. During high-temperature sintering, Sn from the

Scheme 1. Activation of Hematite Photoanodes by High-Temperature Sintering Entails a Kinetic Competition between Sn Dopant Diffusion from the FTO Substrate into the Hematite, and the Resulting Thermal Deformation and Conductivity Loss in the FTO Substrate



FTO substrates diffuses into the hematite lattice, enhancing the PEC properties of the hematite photoanodes. The PEC performance correlated well with the degree of Sn diffusion and EIS data. The Sn diffusion also changes the stoichiometry of the FTO substrates, affecting their conductivity and thus the overall device performance. A sudden drop of photocurrent was observed in hematite nanorods sintered at 800 °C when the sintering time was increased to the longest duration studied (20 min); this was ascribed to the considerably increased resistivity caused by deformation of the FTO substrate. When sintered at high temperature, the diffused Sn atoms from the FTO substrates affected the metal site of the hematite lattice from EXAFS analysis. Increased diffusion of Sn into the hematite lattice disorders its structure, but optimum sintering time compensates for the structural disordering and improves the ordering. Therefore, there is a trade-off between Sn diffusion into the hematite lattice and loss of Sn in the FTO substrate, which considerably degrades the FTO layer and makes it insulating.

■ ASSOCIATED CONTENT

S Supporting Information

Information on XPS, FESEM, PEC optimization, and EIS of 800 °C sintered FTO substrates, along with XPS elemental composition of 800 °C sintered FTO substrates and hematite photoanodes. This material is available free of charge via the Internet at <http://pubs.acs.org>.

■ AUTHOR INFORMATION

Corresponding Author

*Tel: +82-63-850-0846. Fax: +82-63-850-0834. E-mail: jangis75@jbnu.ac.kr.

Notes

The authors declare no competing financial interest.

■ ACKNOWLEDGMENTS

This research was supported by the Basic Science Research Program of the National Research Foundation of Korea (NRF),

funded by the Ministry of Education, Science and Technology (2012R1A6A3A04038530).

■ REFERENCES

- Gratzel, M. Photoelectrochemical Cells. *Nature* **2001**, *414*, 338–344.
- Fujishima, A.; Honda, K. Electrochemical Photolysis of Water at a Semiconductor Electrode. *Nature* **1972**, *238*, 37–38.
- Li, Z.; Luo, W.; Zhang, M.; Feng, J.; Zou, Z. Photoelectrochemical Cells for Solar Hydrogen Production: Current State of Promising Photoelectrodes, Methods to Improve Their Properties, and Outlook. *Energy Environ. Sci.* **2013**, *6*, 347–370.
- Liu, C.; Dasgupta, N. P.; Yang, P. Semiconductor Nanowires for Artificial Photosynthesis. *Chem. Mater.* **2014**, *26*, 415–422.
- Bassi, P. S.; Gurudayal; Wong, L. H.; Barber, J. Iron Based Photoanodes for Solar Fuel Production. *Phys. Chem. Chem. Phys.* **2014**, *16*, 11834–11842.
- Cho, I. S.; Lee, C. H.; Feng, Y.; Logar, M.; Rao, P. M.; Cai, L.; Kim, D. R.; Sinclair, R.; Zheng, X. Codoping Titanium Dioxide Nanowires with Tungsten and Carbon for Enhanced Photoelectrochemical Performance. *Nat. Commun.* **2013**, *4*, 1–8.
- Lin, Y.-G.; Hsu, Y.-K.; Chen, Y.-C.; Chen, L.-C.; Chen, S.-Y.; Chen, K.-H. Visible-Light-Driven Photocatalytic Carbon-Doped Porous ZnO Nanoarchitectures for Solar Water-Splitting. *Nanoscale* **2012**, *4*, 6515–6519.
- Wang, G.; Ling, Y.; Wang, H.; Yang, X.; Wang, C.; Zhang, J. Z.; Li, Y. Hydrogen-Treated WO₃ Nanoflakes Show Enhanced Photo-stability. *Energy Environ. Sci.* **2012**, *5*, 6180–6187.
- Sivula, K. Metal Oxide Photoelectrodes for Solar Fuel Production, Surface Traps, and Catalysis. *J. Phys. Chem. Lett.* **2013**, *4*, 1624–1633.
- Sivula, K.; Le Formal, F.; Graetzel, M. Solar Water Splitting: Progress Using Hematite (α -Fe₂O₃) Photoelectrodes. *ChemSusChem* **2011**, *4*, 432–449.
- Cornell, R. M.; Schwertmann, U. *The Iron Oxides: Structure, Properties, Reactions, Occurrences and Uses*; Wiley: Weinheim, Germany, 2003; Vol. 2.
- Iordanova, N.; Dupuis, M.; Rosso, K. M. Charge Transport in Metal Oxides: A Theoretical Study of Hematite α -Fe₂O₃. *J. Chem. Phys.* **2005**, *122*, 144305–144314.
- Ling, Y.; Wang, G.; Wheeler, D. A.; Zhang, J. Z.; Li, Y. Sn-Doped Hematite Nanostructures for Photoelectrochemical Water Splitting. *Nano Lett.* **2011**, *11*, 2119–2125.
- Jang, J. S.; Lee, J.; Ye, H.; Fan, F.-R. F.; Bard, A. J. Rapid Screening of Effective Dopants for Fe₂O₃ Photocatalysts with Scanning Electrochemical Microscopy and Investigation of Their Photoelectrochemical Properties. *J. Phys. Chem. C* **2009**, *113*, 6719–6724.
- Palomares, E.; Clifford, J. N.; Haque, S. A.; Lutz, T.; Durrant, J. R. Control of Charge Recombination Dynamics in Dye Sensitized Solar Cells by the Use of Conformally Deposited Metal Oxide Blocking Layers. *J. Am. Chem. Soc.* **2003**, *125*, 475–482.
- Hudaya, C.; Park, J. H.; Lee, J. K. Effects of Process Parameters on Sheet Resistance Uniformity of Fluorine-Doped Tin Oxide Thin Films. *Nanoscale Res. Lett.* **2012**, *7*, 1–5.
- Kim, J. Y.; Magesh, G.; Youn, D. H.; Jang, J.-W.; Kubota, J.; Domen, K.; Lee, J. S. Single-Crystalline, Wormlike Hematite Photoanodes for Efficient Solar Water Splitting. *Sci. Rep.* **2013**, *3*, 1–8.
- Morrish, R.; Rahman, M.; MacElroy, J. M. D.; Wolden, C. A. Activation of Hematite Nanorod Arrays for Photoelectrochemical Water Splitting. *ChemSusChem* **2011**, *4*, 474–479.
- Sivula, K.; Zboril, R.; Le Formal, F.; Robert, R.; Weidenkaff, A.; Tucek, J.; Frydrych, J.; Graetzel, M. Photoelectrochemical Water Splitting with Mesoporous Hematite Prepared by a Solution-Based Colloidal Approach. *J. Am. Chem. Soc.* **2010**, *132*, 7436–7444.
- Vayssières, L.; Beermann, N.; Lindquist, S. E.; Hagfeldt, A. Controlled Aqueous Chemical Growth of Oriented Three-Dimensional Crystalline Nanorod Arrays: Application to Iron(III) Oxides. *Chem. Mater.* **2001**, *13*, 233–235.

- (21) Atkinson, A.; Taylor, R. I. Diffusion of Fe⁻⁵⁵ in Fe₂O₃ Single-Crystals. *J. Phys. Chem. Solids* **1985**, *46*, 469–475.
- (22) Gualtieri, A. F.; Venturelli, P. In Situ Study of the Goethite-Hematite Phase Transformation by Real Time Synchrotron Powder Diffraction. *Am. Mineral.* **1999**, *84*, 895–904.
- (23) Ravel, B.; Newville, M. Athena, Artemis, Hephaestus: Data Analysis for X-Ray Absorption Spectroscopy Using Ifeffit. *J. Synchrotron Radiat.* **2005**, *12*, 537–541.
- (24) Xi, L.; Chiam, S. Y.; Mak, W. F.; Tran, P. D.; Barber, J.; Loo, S. C. J.; Wong, L. H. A Novel Strategy for Surface Treatment on Hematite Photoanode for Efficient Water Oxidation. *Chemical Science* **2013**, *4*, 164–169.
- (25) Rehr, J. J.; Kas, J. J.; Prange, M. P.; Sorini, A. P.; Takimoto, Y.; Vila, F. Ab Initio Theory and Calculations of X-Ray Spectra. *C. R. Phys.* **2009**, *10*, 548–559.
- (26) Wyckoff, R. W. G. *Crystal Structures*; Wiley: New York, 1986.
- (27) Blake, R. L.; Hessevic.Re; Zoltai, T.; Finger, L. W. Refinement of Hematite Structure. *Am. Mineral.* **1966**, *51*, 123–129.
- (28) Longo, C.; Freitas, J.; De Paoli, M. A. Performance and Stability of TiO₂/Dye Solar Cells Assembled with Flexible Electrodes and a Polymer Electrolyte. *J. Photochem. Photobiol., A* **2003**, *159*, 33–39.
- (29) Lopes, T.; Andrade, L.; Ribeiro, H. A.; Mendes, A. Characterization of Photoelectrochemical Cells for Water Splitting by Electrochemical Impedance Spectroscopy. *Int. J. Hydrogen Energy* **2010**, *35*, 11601–11608.
- (30) Teesetsopon, P.; Kumar, S.; Dutta, J. Photoelectrode Optimization of Zinc Oxide Nanoparticle Based Dye-Sensitized Solar Cell by Thermal Treatment. *Int. J. Electrochem. Sci.* **2012**, *7*, 4988–4999.